HHS Public Access

Author manuscript

Magn Reson Med. Author manuscript; available in PMC 2018 December 01.

Published in final edited form as:

Magn Reson Med. 2017 December ; 78(6): 2136–2148. doi:10.1002/mrm.26577.

Imaging and T_2 Relaxometry of Short-T_2 Connective Tissues in the Knee using Ultrashort Echo-Time Double-Echo Steady-State (UTEDESS)

Akshay S. Chaudhari[1,2], **Bragi Sveinsson**[1,3], **Catherine J. Moran**[1], **Emily J. McWalter**[4], **Ethan M. Johnson**[3], **Tao Zhang**[1,3], **Garry E. Gold**[1,2], and **Brian A. Hargreaves**[1,2,3]

[1]Department of Radiology, Stanford University, Stanford, California, USA

[2]Department of Bioengineering, Stanford University, Stanford, California, USA

[3]Department of Electrical Engineering, Stanford University, Stanford, California, USA

[4]Department of Mechanical Engineering, University of Saskatchewan, Saskatoon, Saskatchewan, Canada

Abstract

Purpose—To develop a radial, double-echo steady-state (DESS) sequence with ultra-short echo-time (UTE) capabilities for T_2 measurement of short-T_2 tissues along with simultaneous rapid, SNR-efficient, and high-isotropic-resolution morphological knee imaging.

Methods—3D radial UTE readouts were incorporated into DESS, termed UTEDESS. Multiple-echo-time UTEDESS was used for performing T_2 relaxometry for short-T_2 tendons, ligaments, and menisci; and for Dixon water-fat imaging. In vivo T_2 estimate repeatability and SNR efficiency for UTEDESS and Cartesian DESS were compared. The impact of coil combination methods on short-T_2 measurements was evaluated via simulations. UTEDESS T_2 measurements were compared to T_2 measurements from Cartesian DESS, multi-echo spin-echo (MESE), and fast spin-echo (FSE).

Results—UTEDESS produced isotropic resolution images with high SNR efficiency in all short-T_2 tissues. Simulations and experiments demonstrated that sum-of-squares coil combinations overestimated short-T_2 measurements. UTEDESS measurements of meniscal T_2 were comparable to DESS, MESE, and FSE measurements while the tendon and ligament measurements were less biased than those from Cartesian DESS. Average UTEDESS T_2 repeatability variation was under 10% in all tissues.

Conclusions—The T_2 measurements of short-T_2 tissues and high-resolution morphological imaging provided by UTEDESS makes it promising for studying the whole knee, both in routine clinical examinations and longitudinal studies.

Correspondence: Akshay Chaudhari, MS, Stanford University, Department of Radiology, The Lucas Center for MR Spectroscopy and Imaging, 1201 Welch Road P064-n, Stanford, CA, 94305, USA, Phone: (714) 204-5705, akshaysc@stanford.edu.

Keywords

Ultrashort Echo Time (UTE); Double Echo Steady State (DESS); Isotropic Resolution; Short-T2; Relaxometry; Osteoarthritis

Introduction

Magnetic resonance imaging (MRI) is a widely used modality in musculoskeletal imaging due its excellent soft-tissue contrast and diagnostic capabilities. A multitude of pathologies can be diagnosed with MRI with its capability of high-resolution imaging with varied contrasts (1,2). However, there are several tissues in the musculoskeletal system, especially in the knee, that exhibit very low T_2 relaxation times (3), which are challenging to image with high signal-to-noise ratio (SNR) and diagnostically viable contrasts. To overcome these challenges, techniques known as ultrashort echo-time (UTE) sequences have been used to achieve echo times of less than 100μs (4,5).

UTE sequences often rely on 3D radial k-space acquisitions as they obviate the need for slice-selection, phase-encoding, or readout dephasing gradients (6). Radial sampling offers isotropic resolution, high sampling efficiency, and excellent motion robustness, which has renewed interest in radial MRI for musculoskeletal applications (6–8). However, despite generating high SNR for short-T_2 musculoskeletal tissues, short echo times (TE) and repetition times (TR) in UTE sequences typically generate images with a proton density (PD) contrast where most tissues appear isointense. Fat saturation can be utilized to enhance tissue contrast in many musculoskeletal applications, however, performing fat saturation in UTE sequences with short scan times, remains challenging (9).

In addition to anatomical detail, MRI can also provide quantitative information regarding the biochemical state of the tissues. One of the most commonly studied quantitative parameters in musculoskeletal MRI is the T_2 relaxation time. In articular cartilage, T_2 has been proposed to be an indicator of the extracellular matrix state, which is sensitive to water and collagen concentrations, as well as tissue anisotropy (2,10,11). Consequently, T_2 mapping can serve as an important marker for therapeutic monitoring of tissue changes during disease progression or recovery (12,13).

Spin-echo (SE) sequences are commonly used to measure T_2 relaxation times. However, even with a multi-echo SE (MESE) acquisition, clinical translation is hampered due to a prohibitively long scan time for this 2D sequence. Faster variations of SE such as fast spin-echo (FSE) have been used commonly, but they have been found to overestimate T_2 values (14,15). The magnetization-prepared angle-modulated partitioned k-space spoiled gradient echo (3D-MAPSS) sequence can measure T_2 but its magnetization preparation can suffer from inherent time-accuracy tradeoffs (16). Fewer preparatory pulses achieve faster scans at the expense of SNR and T_2* decay-induced k-space modulation. In a recent study comparing various T_2 measurement techniques in articular cartilage (17), the 3D quantitative double-echo steady-state sequence (DESS) (18) allowed for rapid scans with a high dynamic range for T_2 measurements that were highly comparable to SE. Despite the myriad of methods available for T_2 quantification, low SNR limits the ability to accurately measure T_2

in short-T_2 tissues (19). Furthermore, phased-array-coil-combination methods such as sensitivity encoding (SENSE) (20) and sum-of-squares (SoS) (21), can limit accuracy of short-T_2 measurements due to varying noise statistics in low-SNR regions (22).

Current research suggests that osteoarthritis (OA) is not just a disease of the cartilage, but rather of the entire joint (23,24). Variations in cartilage T_2 have been shown to distinguish between healthy subjects and patients with varying degrees of OA, even before the onset of gross morphological changes (25). The short-T_2 menisci, tendons, and ligaments, are integral in joint mechanics and abnormalities in these tissues may impact joint degradation and the onset of OA (23,24,26). Therefore, evaluating T_2 variations in these tissues, between healthy subjects and patients with OA, may help provide sensitive markers for early OA diagnoses. While T_2* has also been linked to identifying OA progression and variations in tissue structure (27), it is sensitive to field inhomogeneities (28) and to chemical shift artifacts (29). Since there exists no consensus suggesting that one parameter is more diagnostically advantageous than the other (28), T_2 measurements were pursued in this study as T_2 might be more clinically robust than T_2*.

In this work, we present a new method termed ultrashort echo-time double-echo steady-state (UTEDESS) that provides T_2 relaxometry for short-T_2 tissues such as menisci, tendons, and ligaments, with high accuracy and precision. We demonstrate how in addition to quantitative imaging, UTEDESS can perform rapid, 3D, SNR-efficient, and high-isotropic resolution imaging in a sequence that provides UTE, T_2, and long-T_2-suppressed contrasts, as well as separate water and fat images. Simulations assess the sensitivity of the T_2 measurements to tissue and imaging parameters, as well to as coil combination methods. We validate the UTEDESS method in vivo in the knee by comparing SNR efficiency with Cartesian DESS, and by comparing UTEDESS T_2 measurements with those from Cartesian DESS and conventional spin echo methods.

Methods

UTEDESS Pulse Sequence

The DESS sequence, which incorporates two readouts separated by a spoiler gradient has been described previously (30–32) and modified to provide T_2 and apparent diffusion coefficient (ADC) measurements (18,33,34). The first echo of DESS (S+) generates a T_1/T_2 contrast common in gradient-spoiled sequences. Following the S+ readout, a spoiler gradient is applied and the second echo (S−) is sampled, which is weighted by both, diffusion and T_2. In this study, “DESS” will always refer to Cartesian DESS.

For UTEDESS, we replaced the DESS Cartesian readouts with 3D radial readouts (Fig. 1a). The S+ echo was sampled with 3D radial-out k-space segments while the S− echo was sampled with complementary radial-in k-space segments, without the need for preparatory or rewinder gradients. A multiple-echo-time version of this sequence was implemented by interleaving two constant duration TRs with two different TEs (Fig. 1c). The signals from the first interleaf were termed S_1+ and S_1−, while those from the second were S_2+ and S_2−. The S_1+ and S_2+ echo times were varied between TE+Δ and an original TE (Δ was a user defined offset). Consequently, the durations between the S_2− and S_1− echo-times and the

following RF pulses were TE+Δ and TE, respectively. All four echoes traversed the same k-space trajectory, albeit in alternating directions for S+ and S−. Such an interleaved TR acquisition with varying echo-times has previously been demonstrated for simultaneous meniscal DESS T_2 and T_2* measurements (35) and for 3D radial steady-state imaging (36).

A non-selective RF pulse and gradient ramp sampling provided a 48μs TE for S_2+. Spoiler gradients (23.5 $mT^1m^{-1}ms^1$ area) were applied on all gradient directions to prevent steady-state banding, minimally sensitizing the S− echoes to diffusion. Water and fat images for both, the S+ and S− echoes, were generated using a flexible-echo-time Dixon water-fat separation method (37,38). The short-T_2 tissue anatomy was highlighted with a long-T_2 subtraction where twice the water S− image was subtracted from the water S+ image (39). Image reconstruction was performed by gridding the 3D radial data onto Cartesian grids (40). A Voronoi cell-based density compensation (41) was used to correct for ramp sampling. A gradient timing delay correction and a B_0 eddy current correction (42) was performed. For a given matrix size NxNxN, πN^2 radial spokes whose endpoints uniformly sample the surface of a sphere (Fig. 1b) were necessary for full Nyquist sampling (compared with N^2 for Cartesian phase encodes). However, radial undersampling does not lead to severe image degradation (43) and we utilized 7x angular undersampling in UTEDESS.

T_2 Mapping

To date, two primary methods have been used in conjunction with DESS to estimate T_2. One method analytically approximates T_2 (33) using the sequence TE and TR, and S−/S+ ratio in Eq. 1, while ignoring flip angle (B_1), T_1 recovery, and diffusion. The second method estimates T_2 by comparing acquired signals to a library of simulated DESS signals with varying T_1, T_2, and ADC values (18,44). In this study, we measured T_2 using an analytical relationship between signals S+ and S− in Eq. 2 (45), based on extended phase graphs (EPG) (46) and UTEDESS timings (Eq. 3).

$$\frac{S-}{S+}=e^{-\frac{2(TR-TE_{S+})}{T_2}} \quad [1]$$

$$\frac{S-}{S+}=e^{-\frac{2(TR-TE_{S+})}{T_2}-(TR-\frac{\tau}{3})\Delta k^2 D}\sin^2\left(\frac{\alpha}{2}\right)\left(\frac{1+e^{(-\frac{TR}{T_1}-TR\Delta k^2 D)}}{1-\cos\alpha e^{-(\frac{TR}{T_1}-TR\Delta k^2 D)}}\right) \quad [2]$$

$$TE_{S-}=2(TR)-TE_{S+} \quad [3]$$

In Eq. 2, α is the flip angle and D is the tissue diffusivity. The spoiler induced dephasing is denoted by $\Delta k=\gamma G\tau$, where G is the spoiler amplitude, τ is the spoiler duration, and γ is the gyromagnetic ratio. Assuming a low diffusion weighting ($\Delta k\approx 0$), a large T_1 relaxation time (T_1 approaches ∞), and a flip angle of 90°, Eqs. 1 and 2 are equivalent. However, for low

flip angles and moderate T_1 values, Eq. 2 greatly improves T_2 accuracy (45). Acquiring separate scans with varying spoiler gradient areas and flip angles can be used for measuring T_2, T_1 and ADC simultaneously. However, non-contrast T_1 is not a commonly used musculoskeletal biomarker while accurate ADC measurements require a minimum of two scans (18,34). For this study, only a single rapid acquisition for T_2 measurement was pursued.

Simulations

The sensitivity of the T_2 fitting procedure to T_1, flip angle, and diffusivity in tendons, menisci, and cartilage (approximate T_2 = 5ms, 12ms, and 35ms, respectively) was evaluated. T_2 for these tissues was simulated with Eq. 2 for T_1 ranging from 0.5s–1.5s, flip angle ranging from 6°–20°, and diffusivity ranging from $0.5\times10^{-9}m^2s^{-1}$ – $2\times10^{-9}m^2s^{-1}$. The error between the original T_2 and the T_2 calculated in this study with Eq. 2 was measured, where all diffusivities were $1.25\times10^{-9}m^2s^{-1}$, all flip angles were 10°, tendon T_1 was 1151ms, meniscus T_1 was 998ms, and cartilage T_1 was 1167ms, as described below.

T_2 measurement variations induced by SoS and SENSE coil combination were explored with Monte Carlo simulations. Tissues with T_2 = 12ms and 30ms, representing meniscus and cartilage respectively, were simulated with spatially varying coil sensitivities and with DESS scan parameters listed in Table 1. Complex Gaussian noise was added to each coil image and coil combination was performed with SoS and R=1 SENSE, commonly referred to as the ‘Roemer’ combination (21), to compare voxel SNR and the estimated T_2 for the two methods.

Volunteer Study

All experiments were performed on a Discovery MR750 3.0T MRI scanner (GE Healthcare, Waukesha, WI) with 50 mT^1m^{-1} maximum gradient amplitudes, $200mT^1m^{-1}ms^{-1}$ maximum slew rates, and a 16-channel receive-only knee coil (Neocoil, Pewaukee, WI). 11 healthy volunteers (five male, age 29±4; six female, age 28±4) were scanned with institutional review board approval and informed consent with a protocol, listed in Table 1, for maximizing short-T_2 signals. DESS and multiple-echo-time UTEDESS were both repeated twice on all volunteers to assess SNR and repeatability of T_2 measurements. Single-slice sagittal 2D MESE and FSE were used to measure T_2 in the medial meniscal using a monoexponential fit (47), for comparisons with UTEDESS T_2 measurements. Low-resolution readouts were used with SE to minimize the TE and echo spacing. However, they could not achieve sufficiently low TEs to accurately characterize tendon and ligament T_2 values so they were used for meniscal T_2 comparisons only. All T_2 measurements were performed with R=1 SENSE coil combinations where coil sensitivity maps were generated by low-pass-filtering the k-space data from the lowest TE scans from every sequence (48).

The meniscus, patellar tendon (PT), and quadriceps tendon (QT) were manually segmented in all scans along with regions of interest of the posterior cruciate ligament (PCL) anterior cruciate ligament (ACL) at their tibial insertion sites. The meniscus was further sub-divided into six sections of the posterior, body, and anterior horns of the medial and lateral meniscus,

to assess regional variation. A PD-weighted fat-saturated FSE (PDw FS FSE) sequence was used to aid in tissue segmentation.

Signal-To-Noise Measurement

SNR was measured in the above regions and the patellar cartilage with DESS and UTEDESS, where UTEDESS slices were downsampled to 3mm. DESS and UTEDESS noise was measured by the "difference method" (7,49). SNR efficiency (η) was calculated for UTEDESS and DESS by normalizing the single-slice SNR with voxel volume and square root of scan time. The tradeoff between S+ SNR and S− contrast-to-noise (CNR) in UTEDESS water was explored by scanning one volunteer with UTEDESS with flip angles of 10°, 15°, 20°, and 30°. Here, SNR was measured in all segmented tissues along with synovial fluid and fat, while CNR was measured between cartilage-fluid, cartilage-meniscus, cartilage-muscle, and cartilage-fat.

T_2 Mapping Data Analysis

UTEDESS and DESS scans were downsampled to an in-plane matrix size of 256×256. Five UTEDESS slices were combined using a complex sum for an effective slice thickness of 3.13mm, comparable to the 3mm slice thicknesses of DESS, MESE, and FSE. The DESS and UTEDESS S−/S+ ratios and Eq. 2 were used to generate pixel-wise T_2 maps in all manually segmented tissues. The multiple-echo-time UTEDESS TE's were: TE_{S1+}=1.10ms, TE_{S2+}=0.05ms, TE_{S1-}=10.90ms, and TE_{S2-}=9.80ms. To measure T_2 in the meniscus, the UTEDESS S_2-/S_1+ echo pairing was used as it produces a higher S− SNR with a lower S_2- TE. For the tendons and ligaments, the S_1-/S_2+ echo pair was used to maximize the S_2+ signal. For illustrative purposes, the difference in T_2 values between a SoS and SENSE approach was performed in a DESS scan. An intra-subject coefficient of variation (CV) was measured (by dividing the T_2 standard deviation across the two scans by its mean) to assess scan-to-scan intra-subject variability for both, DESS and UTEDESS.

A magnetization-prepared rapid gradient-echo imaging (MP-RAGE) sequence (50,51) was used to measure the T_1 values of the segmented tissues, as well as the gastrocnemius muscle and the patellar cartilage for measurement validation, in two volunteers. A Bloch-Siegert B_1 map (52) was acquired to account for possible flip angle variations. T_2 was calculated using the measured T_1 and an approximate diffusivity of $1.25\times10^{-9}m^2s^{-1}$, for both, the nominal flip angle and the measured flip angle. Image reconstruction, signal simulation, and parameter fitting was performed using MATLAB (MathWorks, Natick, MA).

Results

Simulations

Simulations of the UTEDESS signal showed that the fitted short-T_2 has minimal sensitivity to diffusivity, low sensitivity to T_1, and moderate sensitivity to B_1 (Fig. 2). The error in T_2 estimation induced due to inaccurate diffusivity, T_1, and B_1, increases as the T_2 of the tissue increases. Fig. 3 indicates that tissues with a longer-T_2 (30ms) show minimal differences between T_2 measurements obtained from SENSE and SoS, while SoS substantially overestimates the true T_2 for low-T_2 (12ms) tissues. This is expected, since SoS coil

combinations have known noise biases that are problematic for T_2 fitting when the signal approaches the noise floor (21).

Volunteer Study

Consistent with simulations, the SoS short-T_2 overestimation in the meniscus, compared to SENSE, can be seen in-vivo with the DESS scan in Fig. 4. The T_2 variation seen between SoS and R=1 SENSE reconstructions is minor in cartilage, but substantial in the meniscus. This result demonstrates the importance of the R=1 SENSE combination, which we used for all subsequent T_2 mapping.

UTEDESS produced T_1-weighted images (S+), higher T_2-weighted images (S−), water-fat separated S+ and S− images, long-T_2-suppressed images, and T_2 maps in tendons, ligaments, and menisci in arbitrary scan planes (Fig. 5). The UTEDESS images had higher signal in the short-T_2 tissues and a comparable signal in the other tissues (Fig. 6 and 7). The higher signal in the tendons and ligaments (arrows, Fig. 6a–b) allowed for the creation of T_2 maps, which was not possible with DESS due to lower SNR (Fig. 6d and Table 2). The UTEDESS images were free of any obvious undersampling artifacts or image distortions that could arise from radial undersampling and gradient imperfections. The spatial resolution and SNR of UTEDESS were adequate to visualize some fascicular structure of the tendons in the S+ water image.

DESS had additional cartilage-fluid contrast in the S− echoes than UTEDESS, likely due to a longer TR and a higher flip angle, which was most apparent in the tibial cartilage (dash-dot arrow, Fig. 6f, 6h). However, the UTEDESS water-fat separation (Fig. 6e–f) helped generate additional fluid contrast. The water S+ images in Fig. 8 indicate that increasing the flip angles decreases meniscus (solid arrows) SNR, a trend consistent with other soft-tissues as well (Fig. 8i). However, in the water S− image (Fig. 8j), increasing the flip angles increases the cartilage-fluid (dotted arrows) CNR due to higher cartilage signal attenuation relative to the fluid. Overall, higher flip angles increase CNR at a cost of decreased SNR.

The MP-RAGE-based T_1 estimates were: meniscus 998±4ms, tendons 1151±37ms, ligaments 1034±25ms, muscle 1392±41ms, and cartilage 1162±13ms. These values were used in the T_2 measurements with DESS and UTEDESS. T_2 measurements, CV, and SNR values, for all segmented tissues are reported in Table 2. T_2 measurements with MESE and FSE in the medial anterior meniscus were 12.4±1.7ms and 11.2±1.4m respectively, while those in the medial posterior meniscus were 12.0±1.4ms and 11.8±1.1m respectively. These showed excellent agreement with the T_2 measurements in the medial meniscus calculated with UTEDESS with DESS. The T_2 measurements from UTEDESS and DESS agreed well in the meniscus, however, for shorter-T_2 tissues such as the tendons and ligaments, DESS overestimated the T_2. The intra-subject repeatability CV in all tissues with UTEDESS was consistently under 10% for all tissues.

Discussion

In this study UTEDESS provided simultaneous quantitative and morphological imaging of the human knee, focusing primarily on short-T_2 tissues. The parameters for UTEDESS were

chosen to provide accurate and repeatable T_2 measurements in menisci, tendons and ligaments. The UTEDESS T_2 measures in the meniscus showed good agreement with conventional T_2 mapping sequences such as MESE, FSE and DESS. Moreover, the 3D radial acquisition generated images with 3D isotropic resolution that allowed reformats in arbitrary scan planes. The multiple-echo-time version of the sequence provided high SNR efficiency with different contrasts such as T_1-weightings in the UTE S+ echoes, T_2-weightings in the S− echoes, water-fat separation in both S+ and S− echoes, and long-T_2 suppression.

Signal-to-Noise Ratios

UTEDESS was able to image the short-T_2 tissues with high-isotropic resolution and high SNR. DESS had a higher cartilage SNR and slightly higher meniscal SNR in the S+ echo, but this was likely due to the longer TR (20ms vs. 6ms) offering additional T_1 recovery and a longer data acquisition window (5.12ms vs. 0.72ms). EPG based simulations showed that tissues with a T_2 of 10ms had a 10–20% higher signal with DESS than UTEDESS for T_1 ranging between 800ms – 1200ms. The data acquisition duration variation should account for 2.7x higher SNR in DESS, but the short TE and TR in UTEDESS increases signal, resulting in comparable overall SNR between the sequences. UTEDESS did have higher S+ SNR in the tendons and ligaments compared to DESS (Fig. 7a) due to shorter TEs.

While the DESS S+ SNR was higher in the meniscus, UTEDESS provided higher S− SNR in the meniscus, tendons, and ligaments (Fig. 7a). Since the T_2 measurement method described in Eq. 2 relies on a two point ratio, the T_2 values are susceptible to the S− SNR, where noise causes T_2 overestimations (19). Thus, despite DESS offering marginally higher S+ meniscal SNR, UTEDESS provides increased robustness for T_2 mapping due to a higher S− SNR.

When the SNR from both sequences is corrected for scan time and voxel volume, UTEDESS outperforms DESS in terms of SNR efficiency (η) for all short-T_2 tissues in both echoes. To achieve a comparable SNR in the short-T_2 tissues, DESS would require 4–16 averages, which is not pragmatic. It should be noted that UTEDESS samples only 70% of k-space that is sampled with DESS, due to the spherical k-space filtering induced by the 3D radial trajectories.

T_2 Measurement

The UTEDESS images had high SNR and thereby could be used for accurate measurements of T_2 in the meniscus, tendons, and ligaments. The SoS method, overestimated the T_2, compared to SENSE, (Fig. 3) due to coil-combination noise biases. Since the T_2 fitting was performed on magnitude images, regions with a low signal had an increased noise bias where the increased signal was mistakenly attributed to a higher T_2. However, since SENSE uses a linear combination of the coil images, the noise remains zero-mean (20,21) after the coil combination, which reduces the noise bias. Compared to the lower-T_2 and SNR meniscus, coil combination minimally affects T_2 values in high-SNR tissues, such as the cartilage, since noise minimally biases the higher-mean signal (Fig. 4).

Although different statistical models accounting for low-SNR have been suggested for use in quantitative imaging, they rely on an accurate measure of the true noise statistics (19,53,54). Background ROIs cannot accurately depict true noise statistics in scans with phased array coils and parallel imaging (49). This makes low-SNR noise corrections challenging to implement clinically within reasonable scan times. An R=1 SENSE coil-combination does not require any additional information and can be performed retrospectively to measure short-T_2 relaxation times without coil combination noise biases. While this study does not perform a comprehensive noise analysis, it tries to address the importance of coil-combination for measuring short-T_2 values with radial undersampling.

T_2 Validation

The accuracy of the T_2 maps was verified by comparing the meniscus T_2 measurements to those obtained with MESE, FSE, and DESS. With SE sequences, the lowest TE should be lower than the T_2 being probed, which is challenging because the T_2 of the meniscus is around 10ms, while that of tendons and ligaments is even lower. Thus, the meniscus T_2 was used as a basis of comparison between the sequences.

The accuracy of the T_2 measurements could also be attributed to the modified exponential fit proposed in Eq. 2. Without accounting for the measured T_1 and flip angle values, the lower signal intensity in the S− echo can be mistakenly attributed to shorter T_2 which can underestimate T_2 by 10–20%. The simulations in Fig. 2 show that the short-T_2 tissues are somewhat insensitive to variations in the diffusivity, T_1, and B_1. The sensitivity to these parameters increases with increasing tissue T_2, however, with higher-T_2 tissues, it becomes easier to characterize the T_1 and diffusivity using other methods. The MP-RAGE T_1 values in muscle and cartilage were consistent with literature (55,56), and they provided an adequate and rapid T_1 estimate for short-T_2 tissues. However, depending on the tradeoff between scan time and T_1 accuracy needed, saturation recovery or variable-flip-angle UTE methods could be employed (57,58).

In the tendons and ligaments, DESS overestimated the T_2 values as compared to UTEDESS (Table 2). The tendons and ligaments in the DESS S− echo had low SNR and approached the noise floor, which may overestimate T_2. FSE can overestimate T_2 by 10% due to stimulated echo effects (16,17). Excluding the first echo from the multi-echo fit may mitigate this problem (47) but doing so significantly increases the lowest TE. Similarly, with MESE, a lowest TE that is shorter than 10ms would have been preferable. The lack of short-TEs made SE sequences insensitive to the fast-decaying short-T_2 components. Similarly, while UTEDESS had a UTE echo, it relied on a two-point fit with a TE_{S-} of over 10ms, which may have failed to capture the fast-decaying components. Thus, the similarity of the meniscal T_2 measurements with all sequences may be explained by the insensitivity to these fast-decaying short-T_2 components.

T_2 maps were generated with both, a nominal B_1, and with a measured B_1. The B_1 variations were low, and due to limited sensitivity of the T_2 estimates to B_1, there were minimal T_2 differences between the nominal and measured flip angles. Consequently, only the T_2 measurements with the nominal flip angles were reported. The only parameter unavailable in the fitting for T_2 was the diffusivity of the tissues. However, as Fig. 2 shows, UTEDESS and

DESS sequences with low spoiling are very minimally sensitive to diffusion where even large variations in ADC only minimally affect the T_2. Thus, an estimate for short-T_2 ADC values, based on cartilage ADC of $1.25\times10^{-9}m^2s^{-1}$ (18,34), was deemed appropriate. The scan-to-scan repeatability CV was consistently lower than 10% in all tissues and was comparable to the DESS CV values, which showed excellent precision.

Tissues in the knee are sensitive to magic angle effects, wherein tissue T_2 is dependent upon its orientation with B_0 (59). The tibial insertion site of the ACL is mostly aligned with the magic angle while the insertion site of the PCL is mostly orthogonal to B_0 (60). Choosing these insertion sites also minimizes the impact of intrasubstance fluid on ACL T_2 measurements. Thus, magic angle could be one of the major causes of higher T_2 values in the ACL than in the PCL. Such effects with DESS T_2 have been reported earlier (61), which should be similar for UTEDESS and SE methods since the magic angle affects the actual tissue T_2. More importantly, however, one major goal for measuring T_2 and other quantitative parameters is to assess longitudinal changes. Since magic-angle-induced changes in T_2 would generally be consistent over time, T_2 is still efficacious in assessing temporal changes.

Overall, with tissue-specific estimates of the T_1 and diffusivity, the T_2 of short-T_2 tissues can be accurately measured with UTEDESS with good repeatability. As this is one of the few in-vivo studies exploring the T_2 values in short-T_2 tissues, normal spatial and longitudinal variations are not yet well known. However, our study indicates that UTEDESS may be a promising tool to study these variations, and to help evaluate new biomarkers of OA progression and response to therapy.

Other Meniscal T_2 Studies

The meniscal T_2 relaxation times for healthy volunteers measured with UTEDESS (on the order of 10–12ms) agree well with the reported measurements in prior studies (62–67). Most of these studies include the use of the 3D-MAPSS sequence. Compared to 3D-MAPSS, UTEDESS provided the ability to create T_2 maps in arbitrary scan planes, at a higher resolution, in lower scan times, and for not only the meniscus, but tendons and ligaments also.

Potential Clinical Utility

Most research applications of DESS, including its usage in the Osteoarthritis Initiative, rely on fat suppression to create contrast for cartilage segmentation and for diagnosing osteophytes, bone cysts, and bone attrition (68). A Dixon DESS sequence, with a shorter TE and TR, could have been used, but the benefit of a slightly shorter TR would have been mitigated due to the inefficiency in sampling four long Cartesian echoes. A sinc or hard pulse excitation without fat saturation could also have been used, but this would lower the image contrast. Thus, DESS with a spectral-spatial RF pulse was utilized in this study as a reference standard and also to evaluate if DESS could be used to study other tissues in the knee joint. For either implementation of DESS, however, UTEDESS offered a much higher sampling efficiency due to the lack of slice-select, phase-encode and rewinder gradients.

The two-point Dixon technique achieved adequate water-fat separation with UTEDESS. With only two echoes necessary, the TEs for all the input images in multiple-echo-time UTEDESS could also be kept low to achieve water-fat separation of even the short-T_2 tissues (Fig. 5c). The longest UTEDESS S+ TE of 1.1ms used in Dixon imaging at 3T, coupled with 0.7ms readouts, provided high signal and minimal blurring in the water image even in the tendons and ligaments. Such short TEs could not be achieved with water selective RF pulses since they are generally several milliseconds long.

The Dixon water-fat separation increased fluid contrast in the water S− images (Fig. 5f), synonymous to contrast provided by T_2-weighted sequences. The bright fluid signal could also be used for detecting inflammation, meniscal and ligament tears, synovitis, cartilage defects, bone marrow lesions, and cysts (69). DESS did achieve a better fluid contrast in the S− echo (Fig. 6f,6h), but this was due to a longer TR and higher flip angle. As can be seen in Fig. 8, there is an inherent tradeoff between short-T_2 tissue signal and bright fluid contrast, primarily as a function of flip angle. As the flip angle is increased, there is reduced stored longitudinal magnetization, which reduces the overall signal (Fig. 8i). Increasing the flip angle from 10° to 30° reduces the meniscus signal in the water S+ images (Fig. 8a–d) but creates cartilage-fluid contrast in the water S− images (Fig. 8e–h) since fluids experience less signal reduction due to their longer T_2. At higher flip angles (Fig. 8f–h), there also appears to be increased contrast between the synovial membrane and fluid. Simulations in Fig. 2c also suggest that higher flip angles may result in lower T_2 sensitivity to B_1. The low flip angle and short-TR in UTEDESS for this study was chosen to maximize short-T_2 tissue signal for accurate T_2 measurements. Future studies could be performed to investigate such scan parameter tradeoffs for quantitative and morphological imaging.

UTEDESS could assist in diagnostic imaging with its 3D isotropic resolution, which allows image reformatting with arbitrary slice thicknesses and orientations. The radial acquisition has also been shown to provide benign appearance of motion artifacts and excellent insensitivity to patient motion due to signal averaging at the center of k-space (70).

Future Work and Limitations

The pulse sequence design and parameter selection for UTEDESS was performed to image short-T_2 tissues with high SNR for accurate T_2 mapping. A high sampling bandwidth of ±250kHz was used to prevent blurring of short-T_2 tissues. This, however, led to minimal cartilage signal decay from the S+ to the S− echoes due to a TR of only 6ms. Decreased bandwidth readouts with a longer TR could potentially be used to trade-off between SNR of short-T_2 tissues and cartilage signal decay between S+ and S−, allow for cartilage T_2 measurements.

Regarding limitations, the volunteer pool for this study comprised only of 11 healthy young-adults, rather than a more typical OA population. Moreover, future studies could further investigate the role of magic angle and biexponential decay models on T_2 measurements, as discussed previously.

Conclusion

In this study, we developed UTEDESS, a new pulse sequence tailored to knee imaging, which provides short-T_2 relaxometry and morphological imaging. UTEDESS imaging was performed to maximize short-T_2 signal for measuring the T_2 relaxation times of menisci, tendons, and ligaments, with good repeatability, by using a noise bias-free R=1 SENSE coil-combination method. The UTEDESS T_2 measurements in the menisci showed excellent agreement with T_2 measurements obtained with DESS, SE sequences, and other studies from literature. This quantitative imaging was performed simultaneously with rapid and high-isotropic-resolution morphological imaging with multiple contrasts and high SNR efficiency. These results suggest that UTEDESS is a promising tool and an efficient technique for quantitative and morphological imaging of whole knee, suitable for routine clinical imaging as well as for longitudinal clinical studies.

Acknowledgments

Grant Support:

NIH AR063643, NIH EB002524, NIH P41 EB015891; NSF DGE-114747, GE Healthcare

The authors thank Drs. Valentina Taviani and Feliks Kogan for useful discussions.

References

1. Reicher MA, Bassett LW, Gold RH. High-resolution magnetic resonance imaging of the knee joint: pathologic correlations. AJR American journal of roentgenology. 1985; 145(5):903–909. [PubMed: 3876748]
2. Mosher TJ. Musculoskeletal imaging at 3T: current techniques and future applications. Magnetic resonance imaging clinics of North America. 2006; 14(1):63–76. [PubMed: 16530635]
3. Robson MD, Gatehouse PD, Bydder M, Bydder GM. Magnetic resonance: an introduction to ultrashort TE (UTE) imaging. Journal of computer assisted tomography. 2003; 27(6):825–846. [PubMed: 14600447]
4. Qian Y, Williams AA, Chu CR, Boada FE. Multicomponent T2* mapping of knee cartilage: technical feasibility ex vivo. Magnetic resonance in medicine. 2010; 64(5):1426–1431. [PubMed: 20865752]
5. Du J, Diaz E, Carl M, Bae W, Chung CB, Bydder GM. Ultrashort echo time imaging with bicomponent analysis. Magnetic resonance in medicine. 2012; 67(3):645–649. [PubMed: 22034242]
6. Chang EY, Du J, Chung CB. UTE imaging in the musculoskeletal system. Journal of magnetic resonance imaging : JMRI. 2015; 41(4):870–883. [PubMed: 25045018]
7. Al saleh H, Hernandez L, Lee KS, Rosas HG, Block WF, Kijowski R. Rapid isotropic resolution cartilage assessment using radial alternating repetition time balanced steady-state free-precession imaging. Journal of magnetic resonance imaging : JMRI. 2014; 40(4):796–803. [PubMed: 24151247]
8. Kijowski R, Blankenbaker DG, Klaers JL, Shinki K, De Smet AA, Block WF. Vastly undersampled isotropic projection steady-state free precession imaging of the knee: diagnostic performance compared with conventional MR. Radiology. 2009; 251(1):185–194. [PubMed: 19221057]
9. Wu Y, Dai G, Ackerman JL, Hrovat MI, Glimcher MJ, Snyder BD, Nazarian A, Chesler DA. Water- and fat-suppressed proton projection MRI (WASPI) of rat femur bone. Magnetic resonance in medicine. 2007; 57(3):554–567. [PubMed: 17326184]
10. Dardzinski BJ, Mosher TJ, Li S, Van Slyke MA, Smith MB. Spatial variation of T2 in human articular cartilage. Radiology. 1997; 205(2):546–550. [PubMed: 9356643]

11. Mosher TJ, Dardzinski BJ. Cartilage MRI T2 relaxation time mapping: overview and applications. Seminars in musculoskeletal radiology. 2004; 8(4):355–368. [PubMed: 15643574]
12. Trattnig S, Mamisch TC, Welsch GH, Glaser C, Szomolanyi P, Gebetsroither S, Stastny O, Horger W, Millington S, Marlovits S. Quantitative T2 mapping of matrix-associated autologous chondrocyte transplantation at 3 Tesla: an in vivo cross-sectional study. Investigative radiology. 2007; 42(6):442–448. [PubMed: 17507817]
13. Welsch GH, Mamisch TC, Domayer SE, Dorotka R, Kutscha-Lissberg F, Marlovits S, White LM, Trattnig S. Cartilage T2 assessment at 3-T MR imaging: in vivo differentiation of normal hyaline cartilage from reparative tissue after two cartilage repair procedures--initial experience. Radiology. 2008; 247(1):154–161. [PubMed: 18372466]
14. Bartlett PA, Symms MR, Free SL, Duncan JS. T2 relaxometry of the hippocampus at 3T. AJNR American journal of neuroradiology. 2007; 28(6):1095–1098. [PubMed: 17569966]
15. Duncan JS, Bartlett P, Barker GJ. Technique for measuring hippocampal T2 relaxation time. AJNR American journal of neuroradiology. 1996; 17(10):1805–1810. [PubMed: 8933861]
16. Pai A, Li X, Majumdar S. A comparative study at 3 T of sequence dependence of T2 quantitation in the knee. Magnetic resonance imaging. 2008; 26(9):1215–1220. [PubMed: 18502073]
17. Matzat SJ, McWalter EJ, Kogan F, Chen W, Gold GE. T2 Relaxation time quantitation differs between pulse sequences in articular cartilage. Journal of magnetic resonance imaging : JMRI. 2015; 42(1):105–113. [PubMed: 25244647]
18. Staroswiecki E, Granlund KL, Alley MT, Gold GE, Hargreaves BA. Simultaneous estimation of T(2) and apparent diffusion coefficient in human articular cartilage in vivo with a modified three-dimensional double echo steady state (DESS) sequence at 3 T. Magnetic resonance in medicine. 2012; 67(4):1086–1096. [PubMed: 22179942]
19. Raya JG, Dietrich O, Horng A, Weber J, Reiser MF, Glaser C. T2 measurement in articular cartilage: impact of the fitting method on accuracy and precision at low SNR. Magnetic resonance in medicine. 2010; 63(1):181–193. [PubMed: 19859960]
20. Pruessmann KP, Weiger M, Scheidegger MB, Boesiger P. SENSE: sensitivity encoding for fast MRI. Magnetic resonance in medicine. 1999; 42(5):952–962. [PubMed: 10542355]
21. Roemer PB, Edelstein WA, Hayes CE, Souza SP, Mueller OM. The NMR phased array. Magnetic resonance in medicine. 1990; 16(2):192–225. [PubMed: 2266841]
22. Graves MJ, Emmens D, Lejay H, Hariharan H, Polzin J, Lomas DJ. T2 and T2* quantification using optimal B1 image reconstruction for multicoil arrays. Journal of magnetic resonance imaging : JMRI. 2008; 28(1):278–281. [PubMed: 18581394]
23. Poole AR. Osteoarthritis as a whole joint disease. HSS journal : the musculoskeletal journal of Hospital for Special Surgery. 2012; 8(1):4–6. [PubMed: 23372516]
24. Hunter DJ. Pharmacologic therapy for osteoarthritis--the era of disease modification. Nature reviews Rheumatology. 2011; 7(1):13–22. [PubMed: 21079644]
25. Dunn TC, Lu Y, Jin H, Ries MD, Majumdar S. T2 relaxation time of cartilage at MR imaging: comparison with severity of knee osteoarthritis. Radiology. 2004; 232(2):592–598. [PubMed: 15215540]
26. Felson DT. Osteoarthritis as a disease of mechanics. Osteoarthritis and cartilage / OARS, Osteoarthritis Research Society. 2013; 21(1):10–15.
27. Williams A, Qian Y, Golla S, Chu CR. UTE-T2 * mapping detects sub-clinical meniscus injury after anterior cruciate ligament tear. Osteoarthritis and cartilage / OARS, Osteoarthritis Research Society. 2012; 20(6):486–494.
28. Baum T, Joseph GB, Karampinos DC, Jungmann PM, Link TM, Bauer JS. Cartilage and meniscal T2 relaxation time as non-invasive biomarker for knee osteoarthritis and cartilage repair procedures. Osteoarthritis and cartilage / OARS, Osteoarthritis Research Society. 2013; 21(10): 1474–1484.
29. Kirsch S, Kreinest M, Reisig G, Schwarz ML, Strobel P, Schad LR. In vitro mapping of 1H ultrashort T2* and T2 of porcine menisci. NMR in biomedicine. 2013; 26(9):1167–1175. [PubMed: 23505140]

30. Bruder H, Fischer H, Graumann R, Deimling M. A new steady-state imaging sequence for simultaneous acquisition of two MR images with clearly different contrasts. Magnetic resonance in medicine. 1988; 7(1):35–42. [PubMed: 3386520]

31. Redpath TW, Jones RA. FADE--a new fast imaging sequence. Magnetic resonance in medicine. 1988; 6(2):224–234. [PubMed: 3367779]

32. Lee SY, Cho ZH. Fast SSFP gradient echo sequence for simultaneous acquisitions of FID and echo signals. Magnetic resonance in medicine. 1988; 8(2):142–150. [PubMed: 3210952]

33. Welsch GH, Scheffler K, Mamisch TC, Hughes T, Millington S, Deimling M, Trattnig S. Rapid estimation of cartilage T2 based on double echo at steady state (DESS) with 3 Tesla. Magnetic resonance in medicine. 2009; 62(2):544–549. [PubMed: 19526515]

34. Bieri O, Ganter C, Scheffler K. Quantitative in vivo diffusion imaging of cartilage using double echo steady-state free precession. Magnetic resonance in medicine. 2012; 68(3):720–729. [PubMed: 22161749]

35. McWalter, E., Gold, G., Alley, M., Hargreaves, BA. T2 and T2* Relaxometry in the Meniscus using a Novel, Rapid Multi-Echo Steady State Sequence. Proceedings of the 21st Annual Meeting of ISMRM; Salt Lake City, Utah. 2013. p. 686

36. Moran CJ, Brodsky EK, Bancroft LH, Reeder SB, Yu H, Kijowski R, Engel D, Block WF. High-resolution 3D radial bSSFP with IDEAL. Magnetic resonance in medicine. 2014; 71(1):95–104. [PubMed: 23504943]

37. Eggers H, Brendel B, Duijndam A, Herigault G. Dual-echo Dixon imaging with flexible choice of echo times. Magnetic resonance in medicine. 2011; 65(1):96–107. [PubMed: 20860006]

38. Zhang T, Chen Y, Bao S, Alley MT, Pauly JM, Hargreaves BA, Vasanawala SS. Resolving phase ambiguity in dual-echo dixon imaging using a projected power method. Magnetic resonance in medicine. 2016

39. Lee YH, Kim S, Song HT, Kim I, Suh JS. Weighted subtraction in 3D ultrashort echo time (UTE) imaging for visualization of short T2 tissues of the knee. Acta radiologica. 2014; 55(4):454–461. [PubMed: 23934936]

40. Jackson JI, Meyer CH, Nishimura DG, Macovski A. Selection of a convolution function for Fourier inversion using gridding [computerised tomography application]. IEEE transactions on medical imaging. 1991; 10(3):473–478. [PubMed: 18222850]

41. Rasche V, Proksa R, Sinkus R, Bornert P, Eggers H. Resampling of data between arbitrary grids using convolution interpolation. IEEE transactions on medical imaging. 1999; 18(5):385–392. [PubMed: 10416800]

42. Brodsky EK, Klaers JL, Samsonov AA, Kijowski R, Block WF. Rapid measurement and correction of phase errors from B0 eddy currents: impact on image quality for non-Cartesian imaging. Magnetic resonance in medicine. 2013; 69(2):509–515. [PubMed: 22488532]

43. Barger AV, Block WF, Toropov Y, Grist TM, Mistretta CA. Time-resolved contrast-enhanced imaging with isotropic resolution and broad coverage using an undersampled 3D projection trajectory. Magnetic resonance in medicine. 2002; 48(2):297–305. [PubMed: 12210938]

44. Heule R, Ganter C, Bieri O. Rapid estimation of cartilage T2 with reduced T1 sensitivity using double echo steady state imaging. Magnetic resonance in medicine. 2014; 71(3):1137–1143. [PubMed: 23666766]

45. Sveinsson, B., Gold, G., Hargreaves, B. Quantification and artifact reduction from simple modeling of DESS signals. Proceedings of the 24th Annual Meeting of ISMRM; Singapore, Singapore. 2016. p. 788

46. Weigel M, Schwenk S, Kiselev VG, Scheffler K, Hennig J. Extended phase graphs with anisotropic diffusion. Journal of magnetic resonance. 2010; 205(2):276–285. [PubMed: 20542458]

47. Maier CF, Tan SG, Hariharan H, Potter HG. T2 quantitation of articular cartilage at 1. 5 T. Journal of magnetic resonance imaging : JMRI. 2003; 17(3):358–364. [PubMed: 12594727]

48. Rahmer J, Bornert P, Groen J, Bos C. Three-dimensional radial ultrashort echo-time imaging with T2 adapted sampling. Magnetic resonance in medicine. 2006; 55(5):1075–1082. [PubMed: 16538604]

49. Dietrich O, Raya JG, Reeder SB, Reiser MF, Schoenberg SO. Measurement of signal-to-noise ratios in MR images: influence of multichannel coils, parallel imaging, and reconstruction filters. Journal of magnetic resonance imaging : JMRI. 2007; 26(2):375–385. [PubMed: 17622966]
50. Mugler JP 3rd, Brookeman JR. Three-dimensional magnetization-prepared rapid gradient-echo imaging (3D MP RAGE). Magnetic resonance in medicine. 1990; 15(1):152–157. [PubMed: 2374495]
51. Kecskemeti S, Samsonov A, Hurley SA, Dean DC, Field A, Alexander AL. MPnRAGE: A technique to simultaneously acquire hundreds of differently contrasted MPRAGE images with applications to quantitative T mapping. Magnetic resonance in medicine. 2015
52. Sacolick LI, Wiesinger F, Hancu I, Vogel MW. B1 mapping by Bloch-Siegert shift. Magnetic resonance in medicine. 2010; 63(5):1315–1322. [PubMed: 20432302]
53. Miller AJ, Joseph PM. The use of power images to perform quantitative analysis on low SNR MR images. Magnetic resonance imaging. 1993; 11(7):1051–1056. [PubMed: 8231670]
54. Dietrich O, Heiland S, Sartor K. Noise correction for the exact determination of apparent diffusion coefficients at low SNR. Magnetic resonance in medicine. 2001; 45(3):448–453. [PubMed: 11241703]
55. Gold GE, Han E, Stainsby J, Wright G, Brittain J, Beaulieu C. Musculoskeletal MRI at 3. 0 T: relaxation times and image contrast. AJR American journal of roentgenology. 2004; 183(2):343–351. [PubMed: 15269023]
56. Jordan CD, Saranathan M, Bangerter NK, Hargreaves BA, Gold GE. Musculoskeletal MRI at 3.0 T and 7. 0 T: a comparison of relaxation times and image contrast. European journal of radiology. 2013; 82(5):734–739. [PubMed: 22172536]
57. Filho GH, Du J, Pak BC, Statum S, Znamorowski R, Haghighi P, Bydder G, Chung CB. Quantitative characterization of the Achilles tendon in cadaveric specimens: T1 and T2* measurements using ultrashort-TE MRI at 3 T. AJR American journal of roentgenology. 2009; 192(3):W117–124. [PubMed: 19234239]
58. Wright P, Jellus V, McGonagle D, Robson M, Ridgeway J, Hodgson R. Comparison of two ultrashort echo time sequences for the quantification of T1 within phantom and human Achilles tendon at 3 T. Magnetic resonance in medicine. 2012; 68(4):1279–1284. [PubMed: 22246857]
59. Xia Y. Magic-angle effect in magnetic resonance imaging of articular cartilage: a review. Investigative radiology. 2000; 35(10):602–621. [PubMed: 11041155]
60. Hayes CW, Parellada JA. The magic angle effect in musculoskeletal MR imaging. Topics in magnetic resonance imaging : TMRI. 1996; 8(1):51–56. [PubMed: 8820094]
61. Monu UD, Jordan CD, Samuelson BL, Hargreaves BA, Gold GE, McWalter EJ. Cluster analysis of quantitative MRI T2 and T1rho relaxation times ofcartilage identifies differences between healthy and ACL-injured individuals at 3T. Osteoarthritis and cartilage / OARS, Osteoarthritis Research Society. 2016; Advanced online publication. doi: 10.1016/j.joca.2016.09.015
62. Calixto NE, Kumar D, Subburaj K, Singh J, Schooler J, Nardo L, Li X, Souza RB, Link TM, Majumdar S. Zonal differences in meniscus MR relaxation times in response to in vivo static loading in knee osteoarthritis. Journal of orthopaedic research : official publication of the Orthopaedic Research Society. 2016; 34(2):249–261. [PubMed: 26223430]
63. Subburaj K, Kumar D, Souza RB, Alizai H, Li X, Link TM, Majumdar S. The acute effect of running on knee articular cartilage and meniscus magnetic resonance relaxation times in young healthy adults. The American journal of sports medicine. 2012; 40(9):2134–2141. [PubMed: 22729505]
64. Subburaj K, Souza RB, Wyman BT, Le Graverand-Gastineau MP, Li X, Link TM, Majumdar S. Changes in MR relaxation times of the meniscus with acute loading: an in vivo pilot study in knee osteoarthritis. Journal of magnetic resonance imaging : JMRI. 2015; 41(2):536–543. [PubMed: 24347310]
65. Rauscher I, Stahl R, Cheng J, Li X, Huber MB, Luke A, Majumdar S, Link TM. Meniscal measurements of T1rho and T2 at MR imaging in healthy subjects and patients with osteoarthritis. Radiology. 2008; 249(2):591–600. [PubMed: 18936315]

66. Zarins ZA, Bolbos RI, Pialat JB, Link TM, Li X, Souza RB, Majumdar S. Cartilage and meniscus assessment using T1rho and T2 measurements in healthy subjects and patients with osteoarthritis. Osteoarthritis and cartilage / OARS, Osteoarthritis Research Society. 2010; 18(11):1408–1416.

67. Stehling C, Luke A, Stahl R, Baum T, Joseph G, Pan J, Link TM. Meniscal T1rho and T2 measured with 3. 0T MRI increases directly after running a marathon. Skeletal radiology. 2011; 40(6):725–735. [PubMed: 21052658]

68. Peterfy CG, Schneider E, Nevitt M. The osteoarthritis initiative: report on the design rationale for the magnetic resonance imaging protocol for the knee. Osteoarthritis and cartilage / OARS, Osteoarthritis Research Society. 2008; 16(12):1433–1441.

69. Hunter DJ, Guermazi A, Lo GH, Grainger AJ, Conaghan PG, Boudreau RM, Roemer FW. Evolution of semi-quantitative whole joint assessment of knee OA: MOAKS (MRI Osteoarthritis Knee Score). Osteoarthritis and cartilage / OARS, Osteoarthritis Research Society. 2011; 19(8): 990–1002.

70. Glover GH, Pauly JM. Projection reconstruction techniques for reduction of motion effects in MRI. Magnetic resonance in medicine. 1992; 28(2):275–289. [PubMed: 1461126]

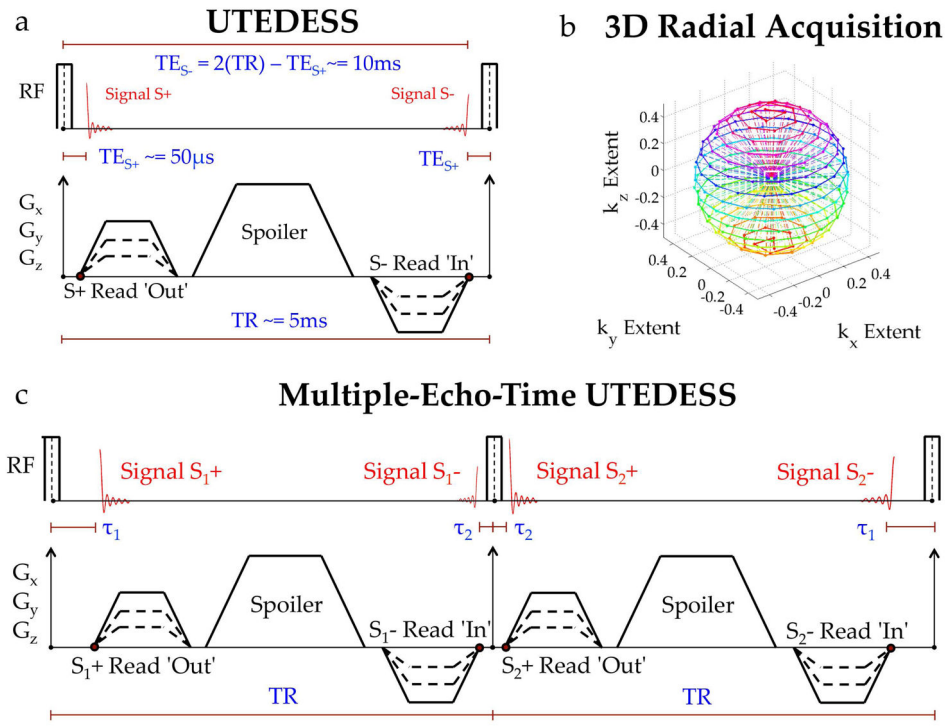

Figure 1.

(a) Illustration of the Ultrashort Echo-Time Double-Echo Steady-State (UTEDESS) pulse sequence. The S+ echo samples the free induction decay caused by the hard RF excitation. The S− echo samples the S+ signal from prior TRs that was dephased and then later rephased. (b) The 3D radial sampling strategy for UTEDESS where the dotted lines represent the trajectory of the radial spokes. The S+ echo is sampled radially outward – from the center of k-space to the radial endpoints (dots on the k-space sphere) while the S− echo is sampled radially inward – from the endpoints to the center of the k-space. (c) A multiple-echo-time version of UTEDESS has gradients in successive TRs shifted by a finite duration while maintaining a constant TR and symmetry across the second RF excitation. This creates a pair of S+ and S− images each with different TEs that can be used for Dixon water-fat separation. The time between S_2− and the subsequent RF pulse can be used for necessary sequence updates, so the Dixon scheme comes at a cost of little sequence dead time.

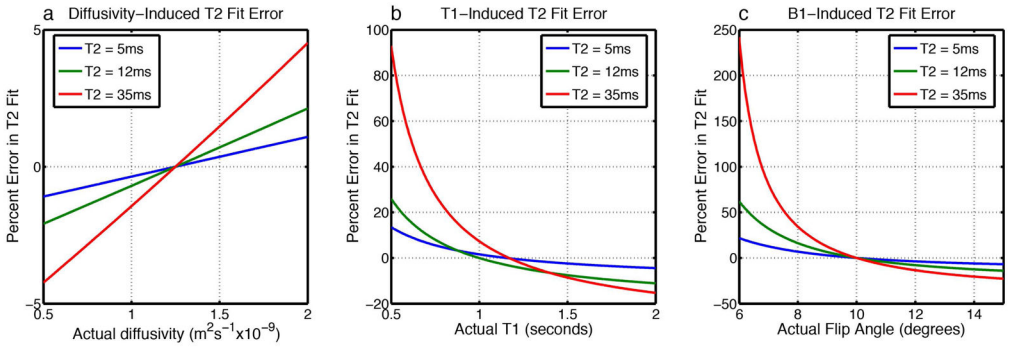

Figure 2.

Sensitivity of the UTEDESS T_2 measurements in tissues with approximate T_2 of tendons (5ms), menisci (12ms), and cartilage (35ms), to parameters of diffusivity, T_1, and B_1. Reference T_2 values were calculated with all diffusivities = $1.25\times10^{-9}m^2s^{-1}$, all flip angles = 10°, tendon T_1 = 1151ms, meniscus T_1 = 998ms, and cartilage T_1 = 1167ms as described below. Simulated T_2 values were calculated with varying diffusivity, T_1, and B1 values, and the error between the reference and simulated values was measured. (a) The sensitivity profile shows minimal sensitivity to ADC, partly because a very low diffusion weighting was applied in the sequence. (b) The short-T_2 tissues show low sensitivity to T_1, where ~40% underestimations in T_1 only lead to ~6% variations in T_2. However, the sensitivity increases as the T_2 of the tissues increases. (c) T_2 measurements show the highest sensitivity to B_1, though the sensitivity decreases significantly with increasing flip angles.

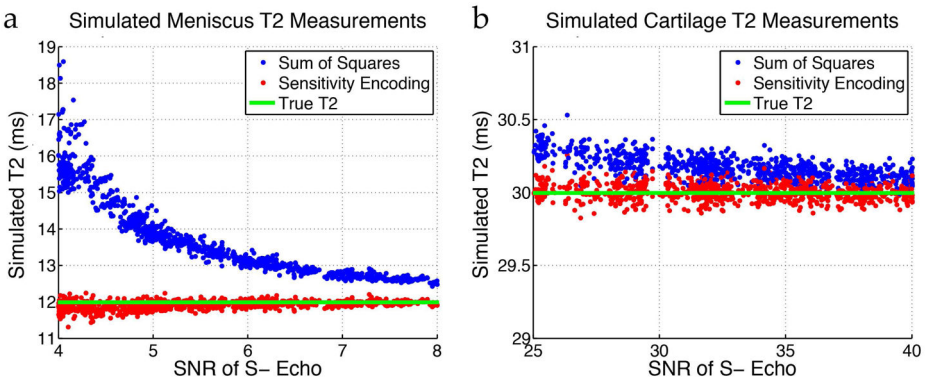

Figure 3.

Monte-Carlo simulations with spatially varying coil sensitivities and varying levels of complex Gaussian noise were performed while using R=1 SENSE and SoS for coil combination and generating T_2 maps. (a) For low SNR values typically seen with meniscus (T_2 about 12ms), SoS significantly overestimates the estimated T_2. (b) For higher SNR typically seen with cartilage (T_2 about 30ms), SENSE and SoS have comparable T_2 estimates.

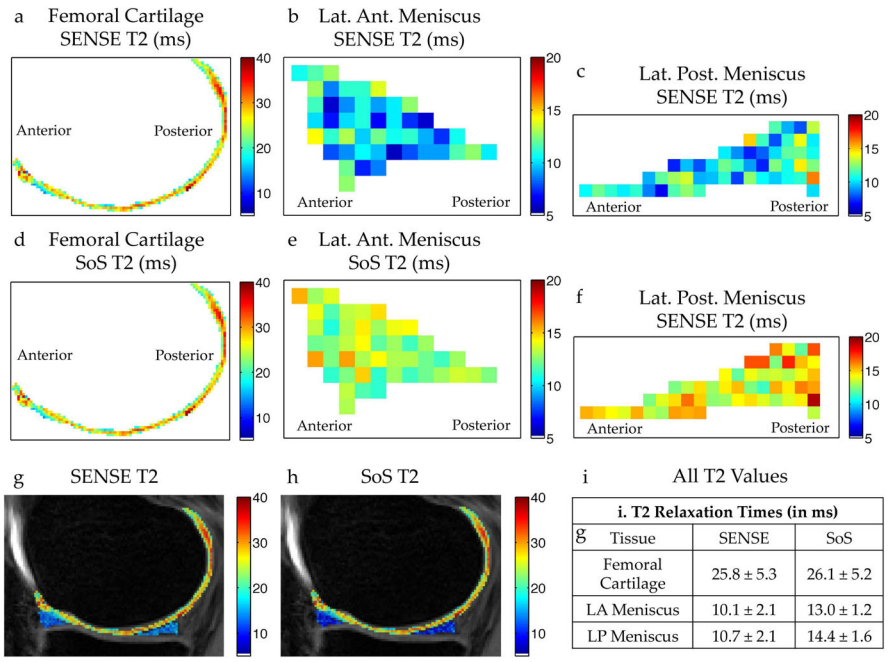

i All T2 Values

i. T2 Relaxation Times (in ms)		
g Tissue	SENSE	SoS
Femoral Cartilage	25.8 ± 5.3	26.1 ± 5.2
LA Meniscus	10.1 ± 2.1	13.0 ± 1.2
LP Meniscus	10.7 ± 2.1	14.4 ± 1.6

Figure 4.

In vivo T_2 differences between R=1 SENSE and SoS coil combinations with DESS. T_2 measurements in the femoral cartilage (a), lateral anterior (LA) meniscal horn (b), and in the lateral posterior (LP) meniscal horn (c) generated with a SENSE coil combination show consistently lower T_2 values in the meniscus compared to a SoS combination for the same regions of interest (d–f). (g–i) Unlike the T_2 in the meniscus, the T_2 measurements in cartilage are similar for both coil combination methods.

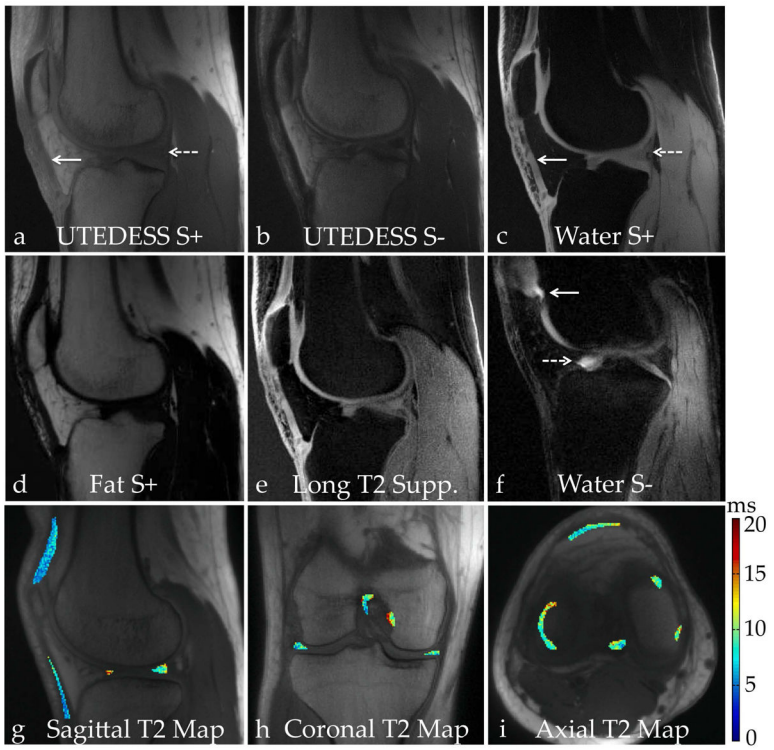

Figure 5.

Images from selected volunteers showing the contrasts that can be generated with UTEDESS. (a) The S+ UTE images are T_1-weighted and have high signal intensity from short-T_2 tissues such as the tendons (solid arrow) and the menisci (dashed arrow). (b) The S − echo is more highly T_2 weighted where the short-T_2 tissues have lower signal. (c) The water-fat separation method provides spectral separation with two echo times. There is clear separation of the short-T_2 tissues of the tendons (solid arrow) and the meniscus (dashed arrow) since the longest echo time used is only 1.1ms. (d) Implementing a Dixon-based water-fat separation, as opposed to using a fat-saturation RF pulse, generates a fat-only image. (e) Performing a weighted subtraction of the water S− image from the water S+ image helps suppress the longer-T_2 signals. This provides a similar contrast to the high SNR water S+ image but the weightings can be modified based on the short-T_2 anatomy that needs to be visualized. (f) In a different subject with fluid in the knee, the water S− image highlights the bright signal around the patellar cartilage (solid arrow) and the anterior horn of the lateral meniscus (dashed arrow). The water S− image has a T_2 weighting and has a lower dynamic range relative to the non-water-fat separated S− image. (g–i) Due to the isotropic resolution of the sequence, the scan planes can be formatted in arbitrary directions to create and view T_2 maps.

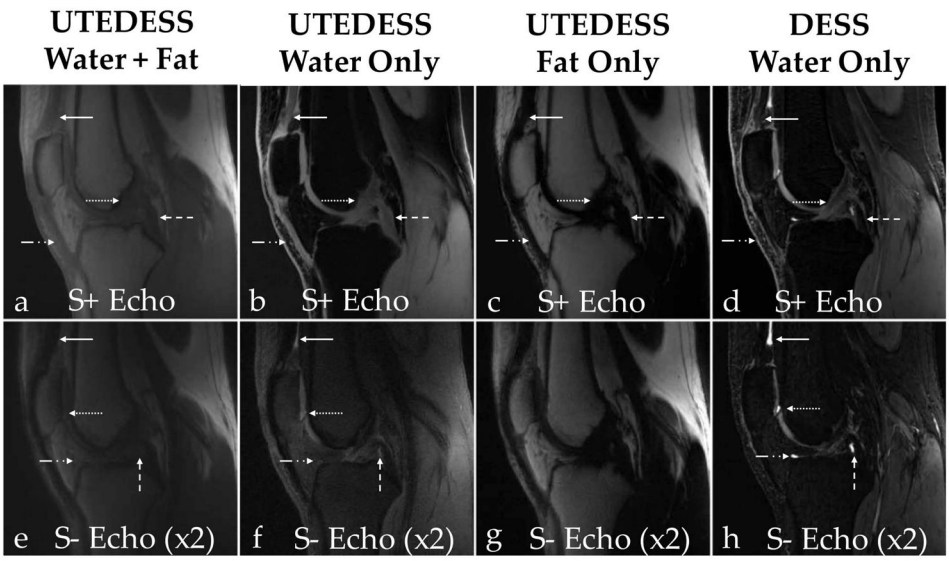

Figure 6.

Comparison of images generated with UTEDESS and DESS. Column 1 shows UTEDESS images, columns 2 and 3 show the UTEDESS retrospective water and fat decomposed images respectively, and column 4 shows the DESS water only acquisition. (a–d) In the S+ images, the quadriceps tendons (solid arrow), patellar tendon (dash-dot arrow), the anterior cruciate ligament (dotted arrow), and the posterior cruciate ligament (dashed arrow) show excellent signal with minimal blurring in the UTEDESS images. There is minimal signal in these tissues with DESS. (e–h) In the S− echoes for both sequences, there is bright fluid signal present posterior to the quadriceps tendon (dashed arrow), in the inferior section of the patellar cartilage (dotted arrow), around the tibial cartilage (dash dot arrow), and the anterior section of the posterior cruciate ligament (dashed arrow). This bright fluid signal can be better visualized with DESS.

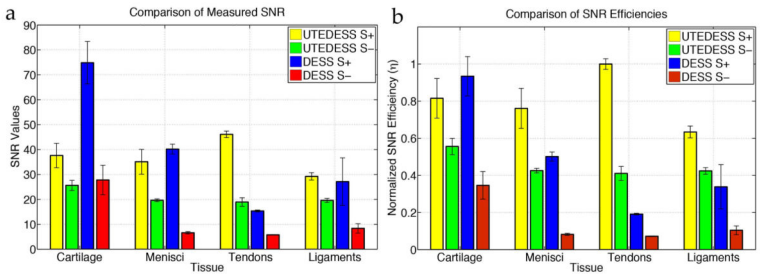

Figure 7.

Comparison of signal-to-noise ratios (SNR) and SNR efficiencies (η) normalized to the scan time and voxel volume. The SNR values (a) show that UTEDESS outperforms DESS in all short-T_2 tissues, except in the S+ echo for meniscus. The S− SNR, however, is higher for all short-T_2 tissues with UTEDESS. This higher SNR makes accurate T_2 fitting possible. (b) The higher SNR efficiencies with UTEDESS show that when normalized for the resolution and scan time, UTEDESS provides a higher SNR in all short-T_2 tissues per unit time, compared to DESS, while maintaining a comparable SNR efficiency in the longer-T_2 tissues such as cartilage.

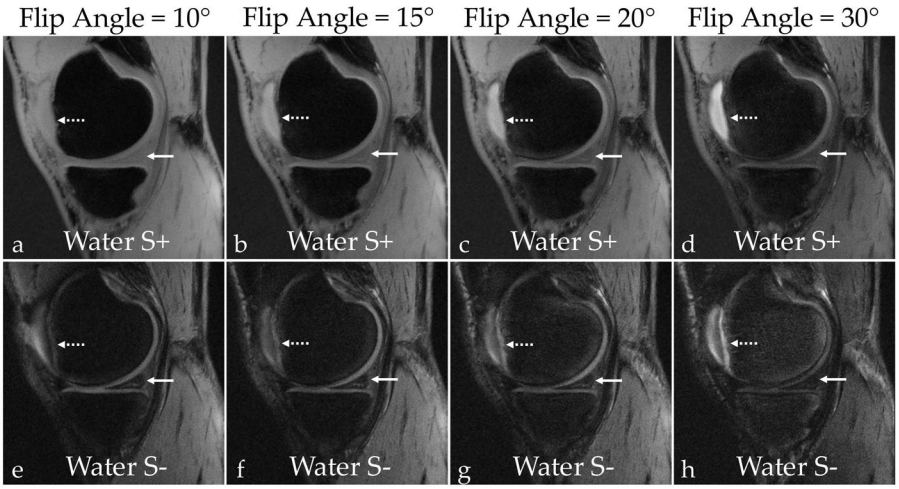

Figure 8.

SNR was measured in the patellar cartilage, the medial meniscus, the patellar tendon, the posterior cruciate ligament, the gastrocnemius muscle, femoral bone marrow (“Fat”), and synovial fluid. (a–d) Increasing the flip angle results in lower signal in the meniscus (solid arrows) in the water S+ images. (e–h) While decreasing overall signal from soft-tissues, higher flip angles also increase cartilage-fluid contrast (dotted arrows) in the water S− images. The increasing flip angle also results in better contrast between the synovial fluid and membrane. (i) By comparing the normalized SNR as a function of flip angle, the SNR for all soft-tissues decreases with an increasing flip angle while the fat and fluid SNR stays relatively constant. (j) An increasing flip-angle increases the cartilage-fluid CNR due to constant fluid signal and attenuated cartilage signals. At a flip of angle of 30°, there is considerably lower meniscal and muscle signal, which reduces the CNR between those tissues and cartilage.

Table 1

Scan protocol for all volunteers in this study. The UTEDESS imaging volume was $(16cm)^3$ while slice thickness for all other sequences were 3mm (except B_1 map which had 6mm thick slices). The legs of volunteers were positioned neutrally, with their right knee being scanned. UTEDESS and DESS were run twice each in order to assess T_2 map reproducibility and tissue SNR. UTEDESS was angularly undersampled by a factor of 7x, to include 45,957 radial spokes.

Sequence	TE (ms)	TR (ms)	Matrix	# Slices	Flip Angle	NEX	Bandwidth (kHz)	Scan Time
UTEDESS	0.05, 1, 10[a], 11[a]	6	320×320	320	10°	1	± 250	8:23×2
DESS	6, 34[a]	20	320×320	40	30°	1	± 31	4:15×2
2D - MESE	10,20,30	2000	128×128	1	90°	0.5	± 31	2:36
2D - FSE	7,14,20,27,33	2000	128×128	1	90°	1	± 31	4:20
B_1 Map	14	30	128×128	20	30°	1	± 15	2:48
PDw FS-FSE	30	3000	384×320	40	111°	2	± 31	3:18
MP-RAGE[b]	3.4	10	256×256	40	4°	1	± 31	3:28×3

[a] UTEDESS and DESS TE_{S-} are longer than the TR since the S− refocusing occurs at 2*TR-TE_{S+}.

[b] MP-RAGE sequences were run on two volunteers with inversion times of 150ms, 1200ms, and 4000ms, in order to assess T_1 relaxation times for the short-T_2 components.

Table 2

T_2 measurements, intra-subject repeatability CVs, and the SNR values for both echoes with UTEDESS and DESS. The reported T_2 values per sequence are averages of the two repeated scans across all volunteers. There is good agreement between T_2 measurements in the meniscus with DESS and UTEDESS, however, DESS overestimates the T_2 of tendons and ligaments, likely due to low-SNR in both echoes. The UTEDESS T_2 measurements show high repeatability with CV values lower than 10%.

	LAM	LBM	LPM	MAM	MBM	MPM	PT	QT	ACL	PCL
UTEDESS										
T_2 (ms)	10.6±1.5	9.7±2.1	9.7±1.5	11.4±1.6	10.9±1.4	10.9±1.8	6.0±1.1	5.2±0.5	9.3±0.8	5.8±0.6
T_2 CV (%)	8.9	8.6	5.8	6.7	6.1	8.0	4.9	6.5	5.6	5.6
S+ SNR	33.1±6.4	35.3±6.1	34.2±5.4	37.8±3.6	35.2±3.9	34.9±4.6	47.0±3.2	45.2±5.8	28.2±3.9	30.2±3.3
S− SNR	19.9±2.1	19.3±3.1	18.8±1.8	20.4±1.7	19.8±1.9	19.6±2.0	20.2±1.9	17.7±2.8	20.1±2.5	19.0±2.3
DESS										
T_2 (ms)	12.1±1.4	12.1±1.3	11.5±1.3	11.6±1.1	12.1±1.3	11.8±1.7	21.0±6.0	12.9±1.4	33.4±6.6	22.3±8.0
T_2 CV (%)	5.7	4.1	4.5	3.1	3.9	4.1	18.6	4.1	6.0	9.2
S+ SNR	39.6±6.6	41.5±6.6	38.7±5.8	43.3±8.7	40.1±5.1	37.9±4.5	15.1±3.3	15.1±2.9	38.7±5.0	19.2±5.5
S− SNR	7.3±1.5	6.4±1.0	7.1±1.8	6.3±1.7	6.3±1.9	6.2±2.0	9.7±1.8	7.0±2.8	13.1±4.2	7.0±1.3

Abbreviations: LAM – lateral anterior meniscus, LBM – lateral meniscus body, LPM – lateral posterior meniscus, MAM – medial anterior meniscus, MBM – medial meniscus body, MPM – medial posterior meniscus, PT – patellar tendon, QT – quadriceps tendon, ACL – anterior cruciate ligament, PCL – posterior cruciate ligament.